Supplemental Material:

Relationship between fill factor and light intensity in solar cells based on organic disordered semiconductors: The role of tail states

Biao Xiao[1], Philip Calado[2], Roderick C. I. MacKenzie[3], Thomas Kirchartz[4,5], Jun Yan[2,*], Jenny Nelson[2]

[1]Key Laboratory of Optoelectronic Chemical Materials and Devices, Ministry of Education, Flexible Display Materials and Technology Co-Innovation Centre of Hubei Province, School of Chemical and Environmental Engineering, Jianghan University, Wuhan, 430056, China.

[2]Department of Physics and Centre for Plastic Electronics, Imperial College London, SW7 2AZ, London, United Kingdom.

[3]Faculty of Engineering, University of Nottingham, University Park, NG7 2RD Nottingham, United Kingdom.

[4]IEK5-Photovoltaics, Forschungszentrum Jülich, 52425 Jülich, Germany

[5]Faculty of Engineering and CENIDE, University of Duisburg-Essen, Carl-Benz-Str. 199, 47057 Duisburg, Germany

Corresponding E-mail: j.yan17@imperial.ac.uk

CONTENTS

I. EXPERIMENTAL SECTION

A. Organic solar cell fabrication

A narrow-bandgap semiconducting polymer poly [[2,6′-4,8-di(5-ethylhexylthienyl) benzo[1,2-b;3,3-b] dithiophene] [3-fluoro-2[(2-ethylhexyl)carbonyl] thieno [3,4-b] thiophenediyl]] (PTB7-Th) [1] is used as the electron donor, and [6,6]-phenyl C_{71}-butyric acid methyl ester ($PC_{71}BM$) and ((5Z,5′Z)-5,5′-(((4,4,9,9-tetraoctyl-4,9-dihydro-s-indaceno[1,2-b:5,6-b′]dithiophene-2,7-diyl) bis(benzo[c][1,2,5]thiadiazole-7,4-diyl)) bis (methanylylidene)) bis (3-ethyl-2-thioxothiazolidin-4-one)) (O-IDTBR) [2] are adopted as the electron acceptors. The ITO substrate with a sheet resistance of 15 Ω sq^{-1} was purchased from CSG HOLDING Co., LTD (China). The device structure was ITO / ZnO / PFN / PTB7-Th: Acceptor / MoO_3 /Ag. Pre-patterned ITO glass substrates were first cleaned using consecutive ultrasonication in acetone, detergent, deionized water, and isopropyl alcohol. The ZnO precursor solution was spin-coated on the ITO-coated glass to form a 30nm electron-transport layer. Then, the ZnO layer was annealed at 200 ºC for 1h in air. After cooling, a thin layer of PFN (5nm) was spin-coated on top of the ZnO layer. PTB7-Th:$PC_{71}BM$ blend was dissolved into a mixed solvent containing 97% Chlorobenzene (CB) and 3% 1,8-Diiodooctane (DIO) with a concentration of 25 mg/ml. PTB7-Th:O-IDTBR blend (24 mg/ml) was dissolved into 1,2-Dichlorobenzene (ODCB) instead. The active layers were spin-coated and thermally annealed at 110 ℃ for 10 min in a N_2-glovebox. Finally, the 10nm MoO_3 hole-transport material and the 70 nm Ag electrode were evaporated through a shadow mask (to define the active area of the devices) in a vacuum (< 10^{-4} Pa).

B. Current-voltage measurement

The current density (J_{sc}), open circuit voltage (V_{oc}), fill factor (FF), and power conversion efficiency (η) values were determined from the current density - voltage *(J-V)* characteristics measured with a Keithley 2450 source-measurement unit under simulated AM 1.5G illumination provided by a solar simulator. The illumination intensity of the simulator was determined using a monocrystalline silicon reference-cell containing a KG-5 visible colour filter.

C. Capacitance measurement

The capacitance-voltage (*C-V*) measurements of the devices were conducted at the room temperature under various light intensities using an impedance analyser (Agilent 4292A). The devices were biased from -2V to 2V and superimposed with AC drive voltage with an oscillating amplitude of 50 mV (rms) in order to maintain the linearity of the response.

II. METHOD SECTION

A. Determination of dark ideality factor from dark current-voltage curves

In general, the *J-V* characteristic of a photodiode can be described by the diode equation with shunt (R_{sh}) and series resistance (R_s):

$$J(V) = J_{ph} - J_0 \cdot \left\{ \exp\left[q \cdot \left(V_{app} + JR_s\right) \Big/ n_{id} k_B T \right] - 1 \right\} - \frac{V_{app} + JR_s}{R_{sh}}, (\mathrm{S2-1})$$

where V_{app} is the externally applied voltage. J_{ph} is the photo-generated current density, J_0 is the reverse saturate current density, and J is the measured current density. The dark current density, J_d can be expressed as

$$J_d = J_0 \cdot \left[\exp\left(q \cdot \left(V_{app} + JR_s\right) \Big/ n_{id,d} k_B T \right) - 1 \right] - \frac{V_{app} + JR_s}{R_{sh}} \ . \quad (\mathrm{S2-2})$$

The dark ideality factor is often extract at the exponential regime of the dark current-voltage plot, as the shunt current density contribution only influences the *J-V* curve in the low applied bias regime, and can be ignored in the exponential regime, therefore in the exponential regime we have

$$J_d = J_0 \cdot \left[\exp\left(q \cdot \left(V_{app} + JR_s\right) \Big/ n_{id,d} k_B T \right) - 1 \right], (\mathrm{S2-3})$$

Therefore,

$$n_{id,d} = \frac{q}{k_B T} \frac{V_{app} + J_d R_s}{\ln(J_d / J_0)}, (S2-4)$$

Series resistance tends to dominate at higher voltages beyond exponential regime and results in a linear (Ohmic) *J-V* regime. Therefore, to avoid influence from series resistive effect, the dark ideality factor $n_{id,d}$ can only be obtained by fitting the exponential regime of the dark current-voltage curves at voltages below the onset of the Ohmic regime, via

$$n_{id,d} = \frac{q}{k_B T} \frac{\partial(V_{app})}{\partial[ln(J_d)]}, (S2-5)$$

B. Determination of light ideality factor from $V_{oc} - Sun$ plot

The light ideality factor is obtained by the slope of $V_{oc} - Sun$ plot. With the device at open circuit no current flows and the series resistance term in the numerator of the exponential goes to zero, and shunt current is much lower than photocurrent (J_{ph}) such that

$$0 = J_{ph} - J_0 \cdot \exp\left(q \cdot V_{oc} \Big/ n_{id,l} k_B T\right). (\mathrm{S2}-6)$$

Assuming J_{ph} is proportional to the light intensity:

$$V_{oc} = n_{id,l} \frac{k_B T}{q} ln\left(\frac{J_{ph}}{J_0}\right) = n_{id,l} \frac{k_B T}{q} ln\left(\frac{C_1 I}{J_0}\right) = n_{id,l} \frac{k_B T}{q} ln(I) + C_2, (S2-7)$$

The light ideality factor $n_{id,l}$ can then be obtained by fitting the $V_{oc} - Sun$ plot.

III. Derivation of the open circuit voltage and internal voltage for direct recombination

The direct recombination rate at open circuit (OC), $R_{rec,dir}(V_{oc})$ can be expressed as

$$R_{rec,dir}(\mathrm{V}_{oc}) = B_{dir} n_{f,oc} p_{f,oc}, (S3-1)$$

Here, the product of free charge density $n_{f,oc}p_{f,oc}$ is determined by the quasi-Fermi level splitting which, in the simplest case, is given by the applied voltage (V_{app}). At open circuit ($V_{app} = V_{oc}$),

$$n_{f,oc}p_{f,oc} = N_C N_V exp\left(-\frac{E_g - qV_{oc}}{k_B T}\right), (S3-2)$$

Where N_C and N_V are the effective density of states for the donor conduction band and acceptor valence band. At OC the generation rate is equal to the recombination rate, hence

$$G = C_G I = B_{dir} n_{f,oc} p_{f,oc} \approx B_{dir} N_C N_V exp\left(-\frac{E_g - qV_{oc}}{k_B T}\right), (S3-3)$$

Therefore, the open circuit voltage (V_{oc}) is can be expressed as

$$V_{oc} = \frac{E_g}{q} - \frac{k_B T}{q} ln\left(\frac{B_{dir} N_C N_V}{C_G I}\right), (S3-4)$$

For a device with contact work functions at the same levels as the band energies, the built-in voltage, V_{bi}, is determined by the effective band gap of the material, $qV_{bi} = E_g$, where E_g is the difference in energy between the Lowest Unoccupied Molecular Orbital (LUMO) of the donor material and the Highest Occupied Molecular Oribtal (HOMO) of the acceptor material in the case of organic bulk heterojunction solar cells. Assuming that the maximum power point (MPP) voltage, V_m is linearly proportional to V_{oc} , such that $V_m = wV_{oc}$, then the internal voltage at MPP, $V_{int,m}$ is given by

$$V_{int,m} = V_{bi} - V_m = \frac{E_g}{q} - wV_{oc} = w\frac{k_B T}{q} ln\left(\frac{B_{dir} N_C N_V}{C_G I}\right) + (1-w)\frac{E_g}{q}. (S3-5)$$

IV. Derivation of trapped and free charge carrier densities

In this section we will consider electrons in the conduction band although analogous solutions can be obtained for holes in the valence band. For a recombination event to occur in the tail state model, a free electron recombines with a trapped hole or a free hole recombines with a trapped electron. We consider the simplest case with symmetric tail slopes below and above the conduction and valence band edges where the tail states start. The total trapped hole density is equal to the total trapped electron density i.e. $p_t = n_t$. Choosing the conduction band to be at zero energy $E_C = 0$, for an exponential-type density of states, the density of electron trapping states per unit energy is giving by

$$g(E) = \frac{N_t}{E_t} exp\left(\frac{E}{E_t}\right), (S4-1)$$

where N_t is the total density of traps, E_t is the characteristic energy that defines the slope of the exponential distribution, and E has negative values. Then the trapped hole and electron density can be expressed as

$$p_t = n_t = \int_{-\infty}^{0} g(E) f(E)\, dE, \qquad (S4-2)$$

where $f(E)$ is the Fermi-Dirac distribution function:

$$f(E) = \frac{1}{exp\left(\frac{E - E_{Fn}}{k_B T}\right) + 1}, (S4-3)$$

where E_{Fn} is the Fermi level for electrons, k_B is the Boltzmann constant, and T is the temperature. Assuming we are at the low temperature limit, $f(E)$ can be approximated as a step function such that

$$f(E) \approx \begin{cases} 1, & E < E_{Fn} \\ 0, & E \geq E_{Fn} \end{cases}, (S4-4)$$

Eq. (S4-2) can then be re-written as

$$p_t = \int_{-\infty}^{E_{Fn}} g(E)\, dE = N_t exp\left(\frac{E_{Fn}}{E_t}\right), (S4-5)$$

For non-zero-energy conduction band edge, we have

$$p_t = N_t exp\left(-\frac{E_C - E_{Fn}}{E_t}\right) = N_t exp\left(-\frac{\Delta E_F}{E_t}\right), (S4-6)$$

where ΔE_F is the relative position of quasi-Fermi level to the conduction band edge.

We evaluate the validity of Eq. (S4-6) by comparing with the numerical results from Eq. (S4-2). As shown in Fig. S1, the agreement is good with characteristic energies larger than 0.03 eV over a range of relative Fermi levels.

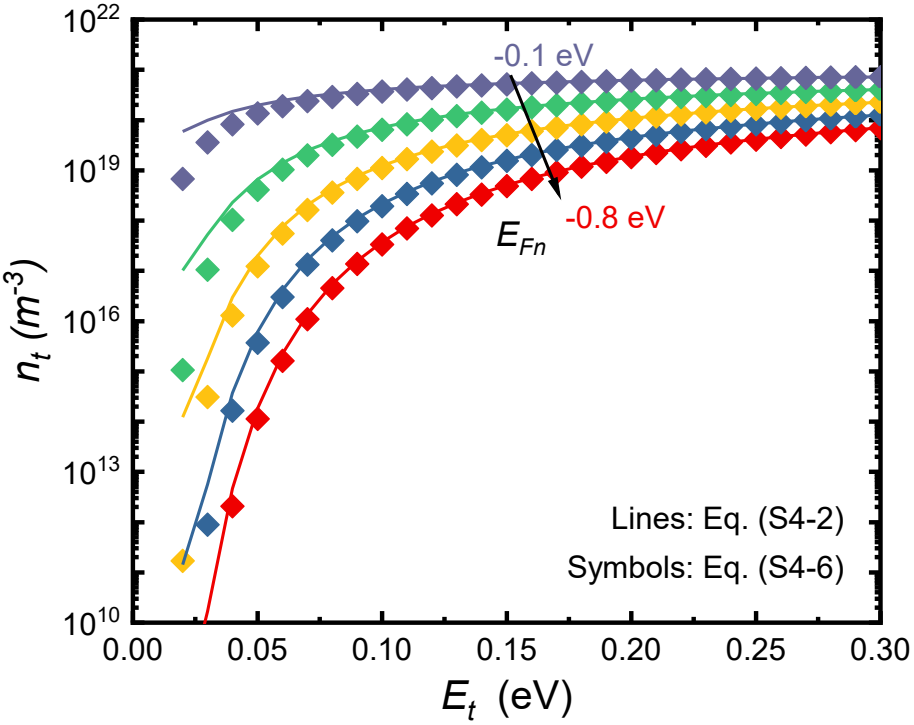

FIG. S1. Comparison between numerical integral from Eq. (S4-2) and analytical expression from Eq. (S4-6) with different Fermi energies. N_t is set to be 10^{21} m^{-3}.

To obtain expressions for the free charge carrier densities we use the commonly applied method of approximating the density of states close to the conduction band edge as a parabolic function. We further assume the quasi Fermi level to be more than several k_BT below E_C. The Fermi-Dirac integral can be approximated by Boltzmann statistics, and the free electron density is given by [3]

$$n_f = N_c exp\left(-\frac{\Delta E_F}{k_B T}\right), (S4-7)$$

V. Derivation of ideality factor, open circuit voltage and internal voltage for trap involved recombination

Assuming that recombination occurs primarily between free and trapped charge carriers, the recombination rate can be written as

$$R_{rec,t} = B_t n_f p_t = B_t \cdot N_t exp\left(-\frac{\Delta E_{Fn}}{E_t}\right) \cdot N_c exp\left(-\frac{\Delta E_{Fn}}{k_B T}\right), (S5-1)$$

At open circuit, assuming ohmic contact, the quasi Fermi level splitting at the contact is equal to the internal quasi Fermi level splitting, and the applied voltage V_{oc}, through

$$E_{Fn,cat} - E_{Fp,ano} = E_{Fn} - E_{Fp} = qV_{oc}, (S5-2)$$

Where $E_{Fn,cat}$ and $E_{Fp,ano}$ are the quasi-Fermi level for electrons and holes at the cathode and anode, respectively. E_{Fn} and E_{Fp} are the internal quasi-Fermi level for electrons and holes, respectively. At OC condition, the quasi Fermi level splitting in the absorber is constant and equal to qV_{oc}. Furthermore, since we assume perfectly symmetric electron and hole DOS and uniform generation, the relative Fermi energy ΔE_F can be then be re-written as

$$\Delta E_F = E_C - E_{Fn} = E_{Fp} - E_V = \frac{1}{2}\left(E_g - qV_{oc}\right), (S5-3)$$

Where E_g is the (effective) band gap of the absorber and E_V is the valence band energy. At open circuit, Eq. (S5-1) therefore becomes

$$R_{rec,t}(V_{oc}) = B_t \cdot N_t exp\left(-\frac{\Delta E_F}{E_t}\right) \cdot N_c exp\left(-\frac{\Delta E_F}{k_B T}\right) = B_t \cdot N_t \cdot N_c \cdot exp\left[-\Delta E_F\left(\frac{1}{E_t}+\frac{1}{k_B T}\right)\right]$$

$$= B_t \cdot N_t \cdot N_c \cdot exp\left[-\frac{1}{2}(E_g - qV_{oc}) \cdot \left(\frac{1}{E_t}+\frac{1}{k_B T}\right)\right]$$

$$= B_t \cdot N_t \cdot N_c \cdot exp\left[-\frac{1}{2}E_g \cdot \left(\frac{1}{E_t}+\frac{1}{k_B T}\right)\right] \cdot exp\left[\frac{1}{2}qV_{oc} \cdot \left(\frac{1}{E_t}+\frac{1}{k_B T}\right)\right]$$

$$= B_t \cdot N_t \cdot N_c \cdot exp\left[-\frac{1}{2}E_g \cdot \left(\frac{1}{E_t}+\frac{1}{k_B T}\right)\right] \cdot exp\left[\frac{qV_{oc}}{k_B T} \cdot \left(\frac{k_B T}{2E_t}+\frac{1}{2}\right)\right]$$

$$\propto exp\left[\frac{qV_{oc}}{k_B T} \cdot \left(\frac{k_B T}{2E_t}+\frac{1}{2}\right)\right]. (S5-4)$$

Therefore, the ideality factor $n_{id,t}$ can be expressed as

$$n_{id,t} = \left(\frac{k_B T}{2E_t}+\frac{1}{2}\right)^{-1}, (S5-5)$$

Since $\alpha = {k_B T}/{E_t} + 1$, we can rewrite Eq. (S5-5) into

$$n_{id,t} = \frac{2E_t}{E_t + k_B T} = \frac{2}{1+\frac{k_B T}{E_t}} = \frac{2}{\Delta}, (S5-6)$$

At open circuit, the volume integral of the recombination rate equals that of the generation rate ($G = C_G I = R_{rec,t}(V_{oc})$). The V_{oc} can then be written as

$$V_{oc} = \frac{n_{id,t}kT}{q}\left[ln\left(\frac{C_G I}{B_t \cdot N_t \cdot N_c}\right)+\frac{1}{2}E_g \cdot \left(\frac{1}{E_t}+\frac{1}{k_B T}\right)\right] = \frac{E_g}{q} - \frac{n_{id,t}kT}{q} ln\left(\frac{B_t N_t N_c}{C_G I}\right). (S5-7)$$

Therefore, since $V_{bi} = \frac{E_g}{q}$, the internal voltage at MPP is given by

$$V_{int,m} = V_{bi} - V_m = \frac{E_g}{q} - wV_{oc} = w\frac{n_{id,t}kT}{q} ln\left(\frac{B_t N_t N_c}{C_G I}\right) + (1-w)\frac{E_g}{q}. (S5-8)$$

VI. Mobility-dependent *FF-Sun* relation under the limit of direct recombination

In the discussion of the *FF-Sun* relation with direct recombination in the main text, the impact of charge transport mobility was neglected. The Schokley-Queisser limit assumes no transport losses, and hence infinite mobility. [4] In this case, *FF* increases marginally with light intensity, as shown in Fig. S2(a) (dashed black line). However, for disordered semiconductor-based solar cells, low mobility is a major concern. To investigate the effects of low mobility, we performed drift-diffusion simulations with varied mobility (Fig. S2(a) (solid lines, square markers)). The base input parameters are the same as in Table S2. For low mobility (< 10^{-1} cm^2 V^{-1} s^{-1}), *FF* becomes negatively dependent on light intensity. This result can be rationalized using an increased transport resistance in the diode equation as shown Fig. S2(b). The simulation results suggest that the often-observed negative *FF-Sun* plot originates from the poor transport mobility.

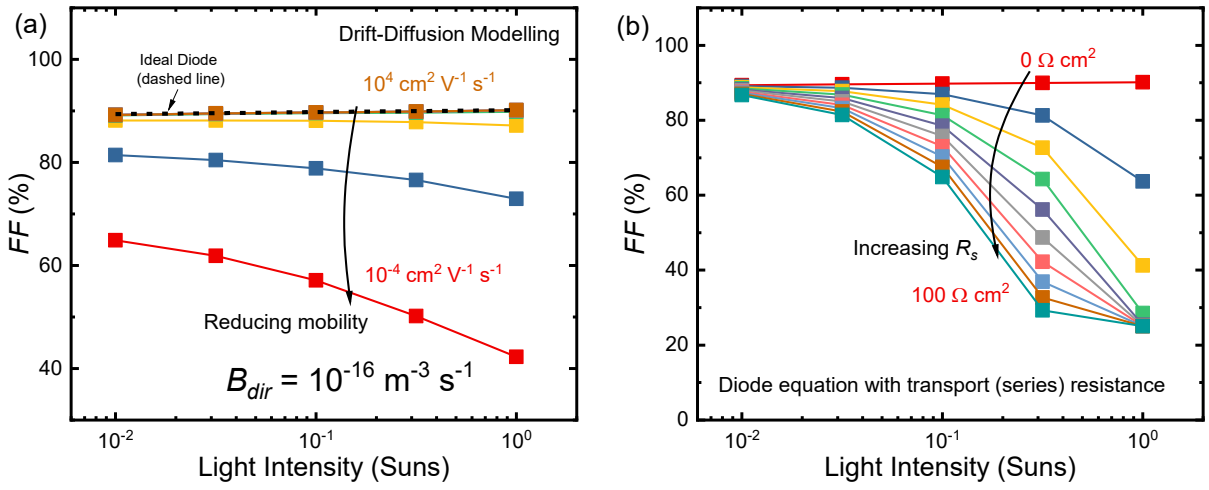

FIG. S2 (a) Drift diffusion modelling: *FF* as a function of light intensity with respect to different mobilities: [10^{-4}, 10^{4}] cm^2 V^{-1} s^{-1}; (b) Diode equation calculations with varied series resistance: [0, 100] Ω cm^2, ideality factor is set to be 1;

VII. Influence of the coefficient of proportionality for the maximum power point and open circuit voltage (w) on the $\Gamma_m - I$ plot

A. Direct recombination

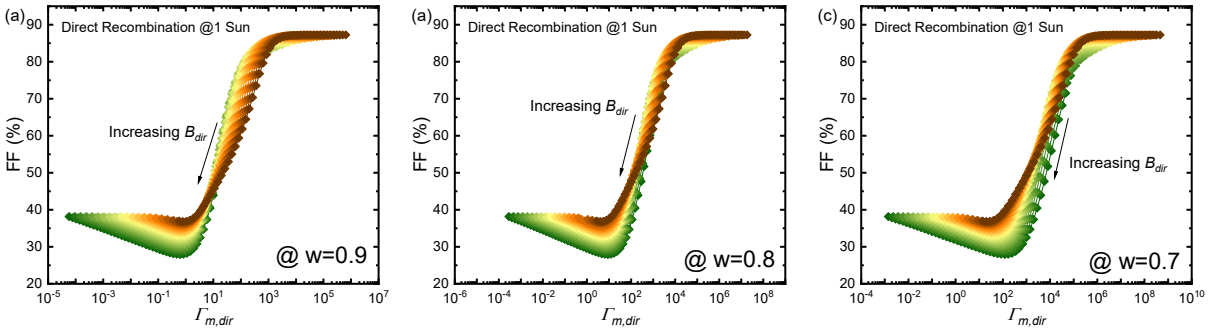

FIG. S3. Simulated FF using gpvdm as a function of calculated $\Gamma_{m,dir}$ for different coefficients of proportionality for the maximum power point and open circuit voltage (w) under 1 Sun illumination. (a) w=0.9; (b) w=0.8; (c) w=0.7. $\Gamma_{m,dir}$ refers to the transport-to-recombination factor limited by direct recombination. Mobility is varied from 10^{-5} (green line) to 10^{-1} cm^2 V^{-1} s^{-1} (brown line).

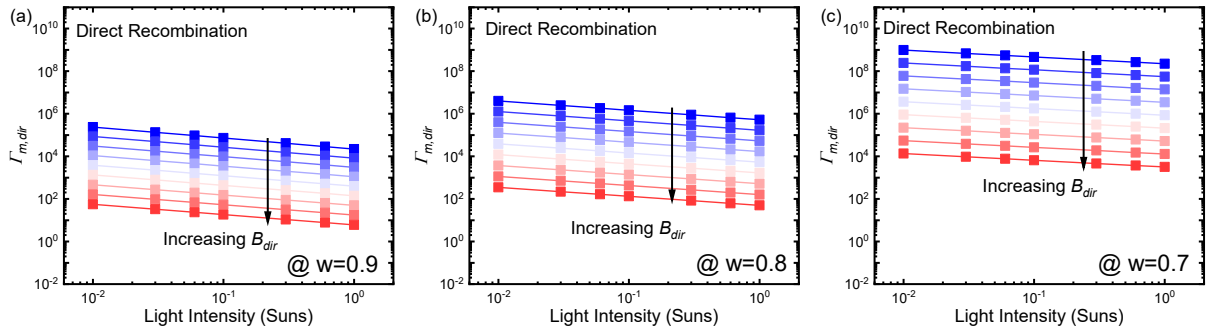

FIG. S4. Calculated $\Gamma_{m,dir}$ as a function of light intensity for different coefficients of proportionality for the maximum power point and open circuit voltage (w). (a) w=0.9; (b) w=0.8; (c) w=0.7. $\Gamma_{m,dir}$ refers to the transport-to-recombination factor limited by direct recombination

B. Tail state mediated recombination

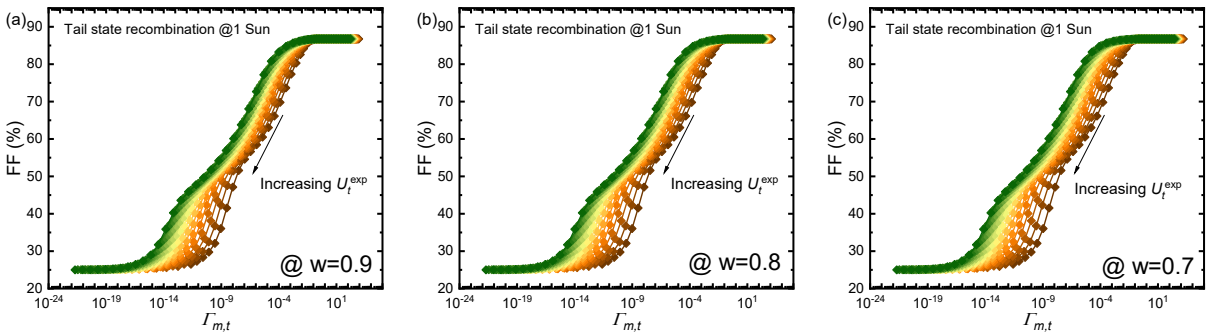

FIG. S5. Simulated FF using gpvdm as a function of calculated $\Gamma_{m,t}$ for different coefficients of proportionality for the maximum power point and open circuit voltage (w) under 1 Sun illumination. (a) w=0.9; (b) w=0.8; (c) w=0.7. $\Gamma_{m,t}$ refers to the transport-to-recombination factor limited by tail state recombination. E_t is varied from 50 meV (brown line) to 150 meV (green line).

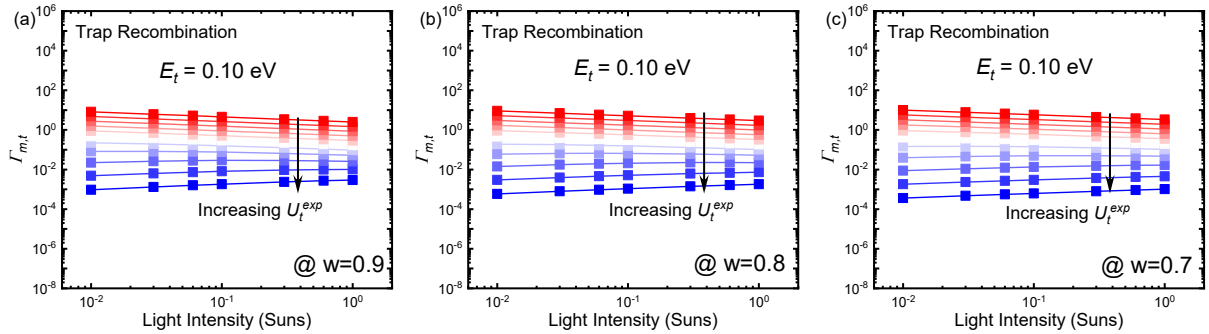

FIG. S6. $\Gamma_{m,t}$ as a function of light intensity for different coefficients of proportionality for the maximum power point and open circuit voltage (w). (a) w=0.9; (b) w=0.8; (c) w=0.7. E_t is set to 0.10 eV for all calculations. $\Gamma_{m,t}$ refers to the transport-to-recombination factor limited by tail state recombination.

VIII. Effect of trapping cross sections in the tail state-mediated recombination model

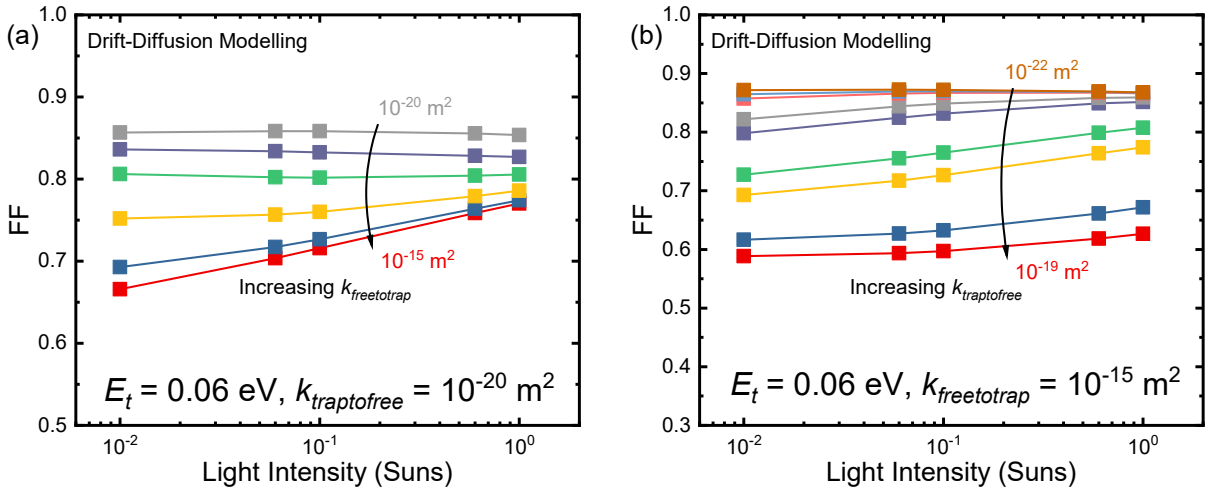

FIG. S7. Effect of trapping cross section. *FF* as a function of light intensity with (a) different free-to-trap (trapping) cross sections and (b) different trap-to-free (recombination) cross sections.

IX. Verifying $V_m - V_{oc}$ relation using gpvdm

Figure S8 shows the simulated voltage at maximum power point (V_m) as a function of open circuit voltage (V_{oc}) using *gpvdm*. [5,6] The parameters for the simulations are listed in Table S3. Specifically, for direct recombination, B_{dir} was set to be 10^{-15} m^3 s^{-1}. For tail state-mediated recombination, E_t was set to be 100 meV, and the effective trap density (U_t^{exp}) was 10^{22} m^{-3} eV^{-1}. Since we are dealing with light intensity-related analysis, the only variable for the simulations was the light intensity, which was changed from 10^{-8} Suns to 1 Sun. Figure S8 shows that the assumption that $V_m \propto V_{oc}$ is reliable for the light intensity dependent analysis for devices limited by either direct or tail state mediated recombination.

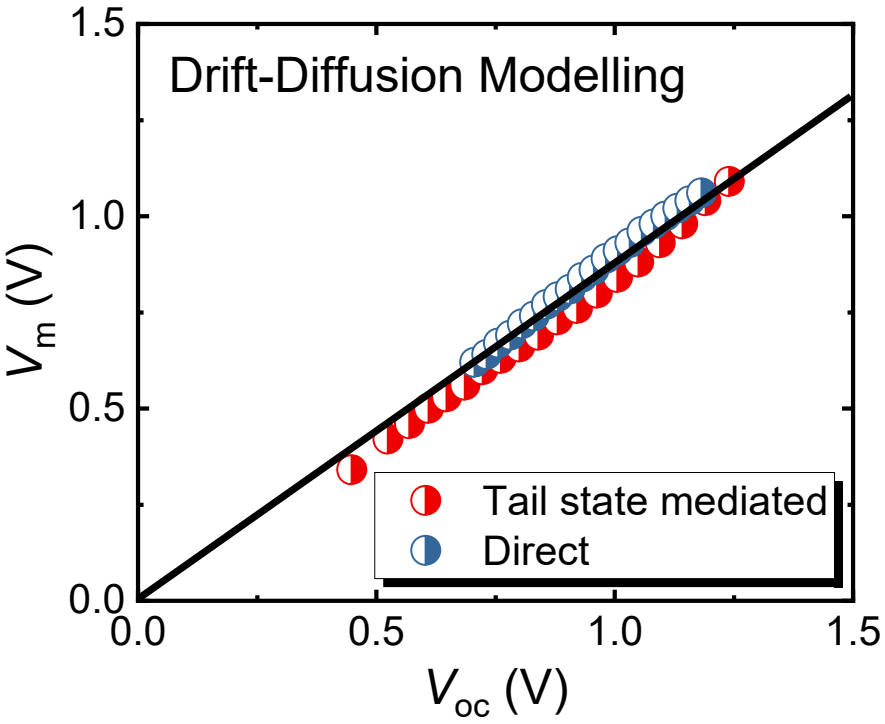

FIG. S8. Calculated voltage at MPP condition (V_m) as a function of open circuit voltage (V_{oc}) using *gpvdm*. Simulations were carried out at light intensities ranging from 10^{-8} Suns to 1 Sun. The solid black line is the fit to the results (circle markers).

X. Effect of contact barriers on *FF-I* relationship

The effect of a contact barrier at the semiconductor-electrode interface on the *FF-I* dependence was studied using drift-diffusion modelling. As shown in FIG. S9a below, when trap states are absent the introduction of contact injection barrier reduces FF at each light intensity, however, the same *FF-I* trend, i.e. negative dependency, is maintained as for the devices without barriers. Fig. S9b shows that the positive dependence of FF on light intensity is only present when traps are involved, and the effect of a contact injection barrier is to reduce the size of the negative FF-I trend. In addition, contact extraction barriers can barely change anything in both trap-free and trap-active cases. Therefore, the presence of contact barriers cannot contribute to a positive *FF-I* dependence.

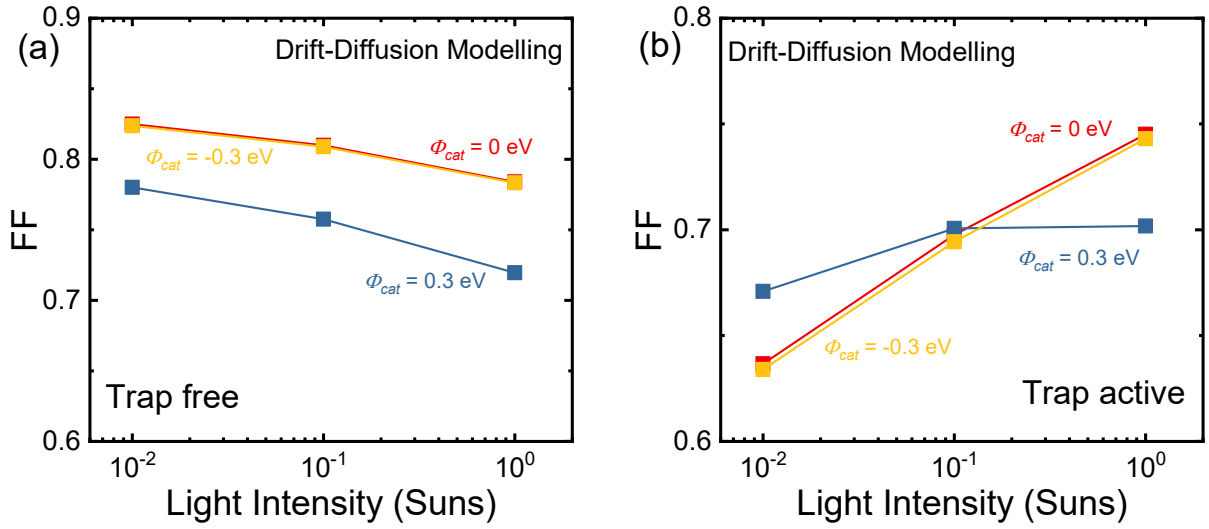

FIG. S9. Effects of contact barrier at cathode on *FF-I* relation under (a) trap free, and (b) trap active condition, simulated using the drift-diffusion model. Specifically, for the trap free device in (a), B_{dir} was set to be 10^{-15} m^3 s^{-1}. For the tail-state active device in (b), E_t was set to be 100 meV, and the effective trap density (U_t^{exp}) was 10^{22} m^{-3} eV^{-1}. $\Phi_{cat} = 0$ eV, 0.3 eV, and -0.3 eV, represent zero, 0.3 eV injection, and 0.3 eV extraction barrier, respectively.

XI. Effect of V_{bi} on *FF-I* relationship

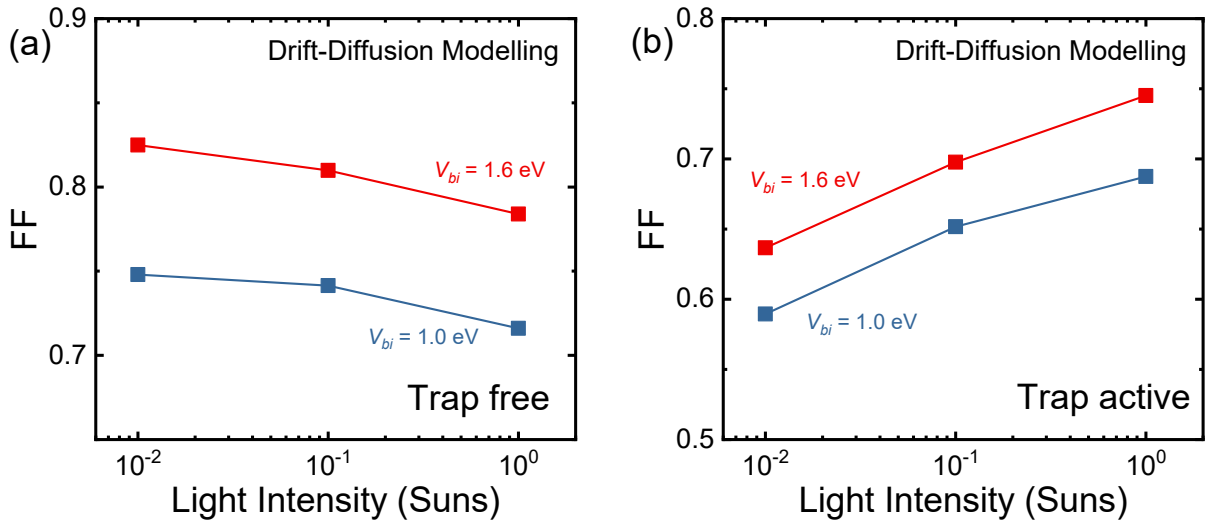

FIG. S10. Effects of built-in potential (V_{bi}) on *FF-I* relation under (a) trap free, and (b) trap active condition, simulated using the drift-diffusion model. Specifically, for the trap free device in (a), B_{dir} was set to be 10^{-15} m^3 s^{-1}. For the tail-state active device in (b), E_t was set to be 100 meV, and the effective trap density (U_t^{exp}) was 10^{22} m^{-3} eV^{-1}. We also assume $E_g = V_{bi}$.

XII. Energy level alignment

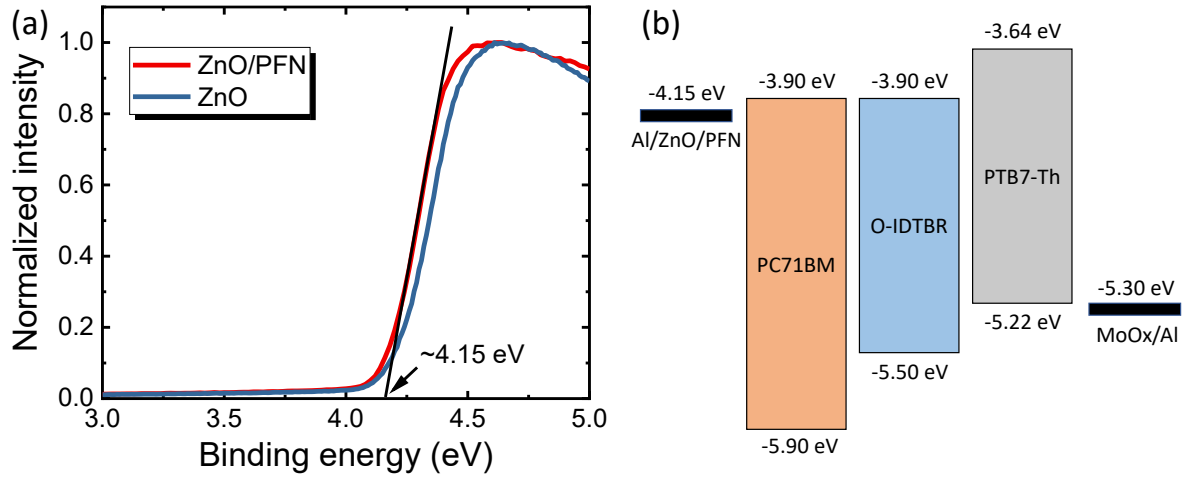

FIG. S11. (a) Work function of ZnO/PFN was determined using ultraviolet photoelectron spectroscopy (UPS) performed on a Thermo-VG Scientific ESCALAB 250 photoelectron spectrometer with incident UV energy of 21.2 eV. (b) Energy level alignment. The work function of MoOx/Al is taken from Ref. [7], energy levels of PC71BM are from Ref. [8–12], energy levels of O-IDTBR are from Ref. [2,13], and energy levels of PTB7-Th are from [14].

XIII. Experimental dark ideality factors

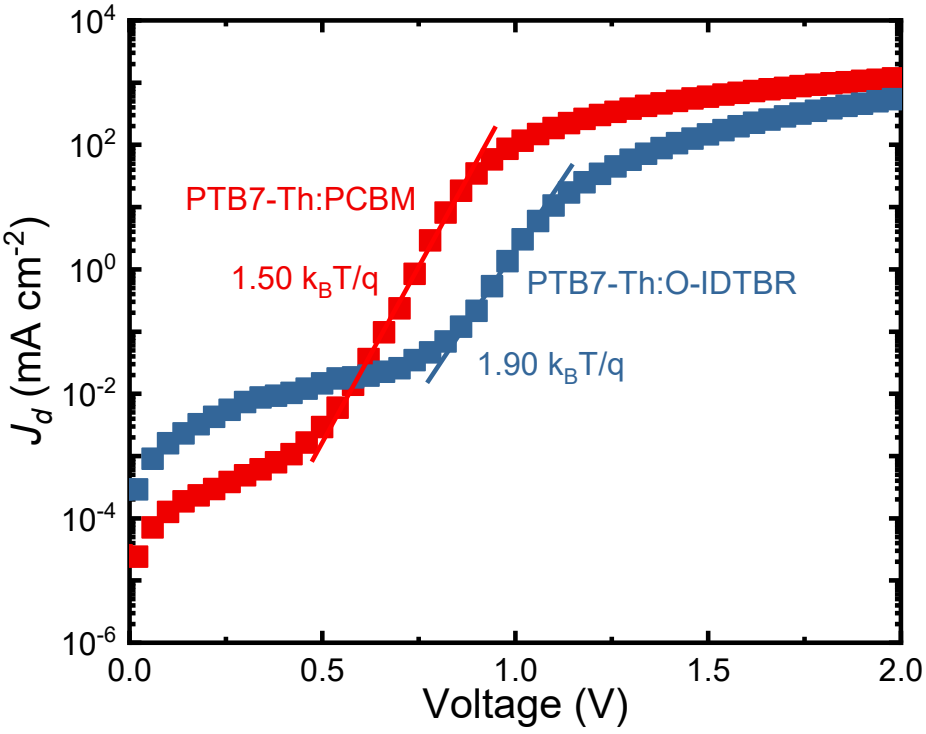

FIG. S12. Dark ideality factors determined from dark *J-V* characteristics of the solar cells. The solid lines are fits to the data indicated by square markers.

TABLE S1. Comparisons between Koster model [15] **and our Tail state-mediated model.** The green shaded rows indicate different assumptions made in the two models while yellow shaded rows indicate the assumptions common to both models.

Key aspects / **Model**	**Koster Model** [15]	**Tail state-mediated model**
Operating condition	Short circuit (SC)	Maximum Power Point (MPP)
Recombination mechanism	Langevin-type-bimolecular	Tail state-mediated
Mobility	Constant	$\mu \propto \frac{n_f}{n_f + n_t}$
Absorption profile	Uniform across the device	Uniform across the device
Charge transport mechanism	Drift-dominated	Drift-dominated
Parameterized by	$\frac{1}{\theta} = K_{dr}/K_{rec}$	$\Gamma_m = K_{dr}/K_{rec}$

TABLE S2. Key parameters input for analytical model Eq. (10).

Parameters	Symbol	Values	Units
Temperature	T	300	K
Active layer thickness	L	100	nm
Effective density of band states for free charge carriers	N_C, N_V	1×10^{25}	m^{-3}
Free carrier mobility	μ	1×10^{-2}	$cm^2\ V^{-1}s^{-1}$
Built-in voltage	V_{bi}	1.6	V
Direct recombination coefficient	B_{dir}	varied	$m^3\ s^{-1}$
Generation rate at 1 sun	C_G	2×10^{28}	$m^{-3}\ s^{-1}$

TABLE S3. Key parameters input for one-dimensional drift-diffusion modelling using gpvdm. [5] The yellow shaded rows indicated parameters used in both direct and trap recombination while the green shaded rows indicate parameters used in the simulation for traps only.

Parameters	Symbol	Values	Units
Temperature	T	300	K
Relative dielectric constant	$\mathcal{E}_r$	4	unitless
Effective density of states of free charges	N_C/N_V	1×10^{25}	m^{-3}
Conduction band energy	E_C	-4.0	eV
Valence band energy	E_V	-5.6	eV
Active layer thickness	L	100	nm
Generation rate at one sun	G	2×10^{28}	$m^{-3}\ s^{-1}$
Cathode electron density	n_l	1×10^{25}	m^{-3}
Anode hole density	p_r	1×10^{25}	m^{-3}
Trap-Free Electron Mobility	μ_n	1×10^{-2}	$cm^2\ V^{-1}s^{-1}$
Trap-Free Hole Mobility	μ_p	1×10^{-2}	$cm^2\ V^{-1}s^{-1}$
Free to free charge recombination coefficient	B_{dir}	Direct: 10^{-19} to 10^{-11} Trap: 0	$m^3\ s^{-1}$
Effective electron trap density	U_e^{exp}	varied	$m^{-3}\ eV^{-1}$
Effective hole trap density	U_h^{exp}	Same as U_e^{exp}	$m^{-3}\ eV^{-1}$
Characteristic energy for electron exponential tail	E_e^u	varied	eV
Characteristic energy for hole exponential tail	E_h^u	Same as E_e^u	eV
LUMO electron capture cross section	σ_e^e	1e-15	m^2
LUMO hole capture cross section	σ_h^e	1e-20	m^2
HOMO electron capture cross section	σ_e^h	1e-20	m^2
HOMO hole capture cross section	σ_h^h	1e-15	m^2

REFERENCES:

[1] Z. He, B. Xiao, F. Liu, H. Wu, Y. Yang, S. Xiao, C. Wang, T. P. Russell, and Y. Cao, *Single-junction polymer solar cells with high efficiency and photovoltage*, Nat. Photonics **9**, 174 (2015).

[2] D. Baran, R. S. Ashraf, D. A. Hanifi, M. Abdelsamie, N. Gasparini, J. A. Röhr, S. Holliday, A. Wadsworth, S. Lockett, M. Neophytou, C. J. M. Emmott, J. Nelson, C. J. Brabec, A. Amassian, A. Salleo, T. Kirchartz, J. R. Durrant, and I. McCulloch, *Reducing the efficiency-stability-cost gap of organic photovoltaics with highly efficient and stable small molecule acceptor ternary solar cells*, Nat. Mater. **16**, 363 (2017).

[3] S. M. Sze and K. K. Ng, *Physics of Semiconductor Devices*, *Physics of Semiconductor Devices* (John Wiley & Sons, Inc., Hoboken, NJ, USA, 2006).

[4] W. Shockley and H. J. Queisser, *Detailed Balance Limit of Efficiency of p-n Junction Solar Cells*, J. Appl. Phys. **32**, 510 (1961).

[5] R. C. I. MacKenzie, *General-purpose Photovoltaic Device Model—gpvdm*, Https://Www.Gpvdm.Com. (n.d.).

[6] R. C. I. MacKenzie, C. G. Shuttle, M. L. Chabinyc, and J. Nelson, *Extracting microscopic device parameters from transient photocurrent measurements of P3HT:PCBM solar cells*, Adv. Energy Mater. **2**, 662 (2012).

[7] R. Xia, D. S. Leem, T. Kirchartz, S. Spencer, C. Murphy, Z. He, H. Wu, S. Su, Y. Cao, J. S. Kim, J. C. Demello, D. D. C. Bradley, and J. Nelson, *Investigation of a conjugated polyelectrolyte interlayer for inverted polymer:fullerene solar cells*, Adv. Energy Mater. **3**, 718 (2013).

[8] L. Zhang, T. Yang, L. Shen, Y. Fang, L. Dang, N. Zhou, X. Guo, Z. Hong, Y. Yang, H. Wu, J. Huang, and Y. Liang, *Toward Highly Sensitive Polymer Photodetectors by Molecular Engineering*, Adv. Mater. **27**, 6496 (2015).

[9] Y. Zhang, D. Deng, K. Lu, J. Zhang, B. Xia, Y. Zhao, J. Fang, and Z. Wei, *Synergistic Effect of Polymer and Small Molecules for High-Performance Ternary Organic Solar Cells*, Adv. Mater. **27**, 1071 (2015).

[10] T. Jiang, J. Yang, Y. Tao, C. Fan, L. Xue, Z. Zhang, H. Li, Y. Li, and W. Huang, *Random terpolymer with a cost-effective monomer and comparable efficiency to PTB7-Th for bulk-*

heterojunction polymer solar cells, Polym. Chem. **7**, 926 (2016).

[11] M.-A. Pan, T.-K. Lau, Y. Tang, Y.-C. Wu, T. Liu, K. Li, M.-C. Chen, X. Lu, W. Ma, and C. Zhan, *16.7%-efficiency ternary blended organic photovoltaic cells with PCBM as the acceptor additive to increase the open-circuit voltage and phase purity*, J. Mater. Chem. A **7**, 20713 (2019).

[12] L. Hu, W. Qiao, J. Qi, X. Zhang, J. Han, and C. Wang, *Significant enhancement of photodetector performance by subtle changes in the side chains of dithienopyrrole-based polymers*, RSC Adv. **6**, 22494 (2016).

[13] S. Holliday, R. S. Ashraf, A. Wadsworth, D. Baran, S. A. Yousaf, C. B. Nielsen, C. H. Tan, S. D. Dimitrov, Z. Shang, N. Gasparini, M. Alamoudi, F. Laquai, C. J. Brabec, A. Salleo, J. R. Durrant, and I. McCulloch, *High-efficiency and air-stable P3HT-based polymer solar cells with a new non-fullerene acceptor*, Nat. Commun. **7**, 1 (2016).

[14] S.-H. Liao, H.-J. Jhuo, Y.-S. Cheng, and S.-A. Chen, *Fullerene Derivative-Doped Zinc Oxide Nanofilm as the Cathode of Inverted Polymer Solar Cells with Low-Bandgap Polymer (PTB7-Th) for High Performance*, Adv. Mater. **25**, 4766 (2013).

[15] D. Bartesaghi, I. del C. Pérez, J. Kniepert, S. Roland, M. Turbiez, D. Neher, and L. J. A. Koster, *Competition between recombination and extraction of free charges determines the fill factor of organic solar cells*, Nat. Commun. **6**, 7083 (2015).